POLITECNICO DI TORINO
Repository ISTITUZIONALE

Comparative Turn-off Safe Modes of Ferrite- and NdFeB- Interior PMSMs

Original
Comparative Turn-off Safe Modes of Ferrite- and NdFeB- Interior PMSMs / Ragazzo, Paolo; Dilevrano, Gaetano; Ferrari, Simone; Pellegrino, Gianmario. - ELETTRONICO. - (2023), pp. 4133-4139. (Intervento presentato al convegno 2023 IEEE Energy Conversion Congress and Exposition (ECCE) tenutosi a Nashville, TN, USA nel 29 October 2023 - 02 November 2023) [10.1109/ECCE53617.2023.10362467].

Availability:
This version is available at: 11583/2985704 since: 2024-02-06T08:09:19Z

Publisher:
IEEE

Published
DOI:10.1109/ECCE53617.2023.10362467

Terms of use:

This article is made available under terms and conditions as specified in the corresponding bibliographic description in the repository

Publisher copyright
IEEE postprint/Author's Accepted Manuscript

©2023 IEEE. Personal use of this material is permitted. Permission from IEEE must be obtained for all other uses, in any current or future media, including reprinting/republishing this material for advertising or promotional purposes, creating new collecting works, for resale or lists, or reuse of any copyrighted component of this work in other works.

(Article begins on next page)

15 January 2025

Comparative Turn-off Safe Modes of Ferrite- and NdFeB- Interior PMSMs

Paolo Ragazzo
Dipartimento Energia Galileo Ferraris
Politecnico di Torino
Turin, Italy
paolo.ragazzo@polito.it

Gaetano Dilevrano
Dipartimento Energia Galileo Ferraris
Politecnico di Torino
Turin, Italy
gaetano.dilevrano@polito.it

Simone Ferrari
Dipartimento Energia Galileo Ferraris
Politecnico di Torino
Turin, Italy
simone.ferrari@polito.it

Gianmario Pellegrino
Dipartimento Energia Galileo Ferraris
Politecnico di Torino
Turin, Italy
gianmario.pellegrino@polito.it

***Abstract*—This paper deals with the analysis of the safe turn-off strategies recommended for permanent magnet synchronous machines. Two common safe state modes are considered: active short circuit, useful to avoid dangerous levels of uncontrolled generator voltages; and active open circuit, which is preferred to avoid abrupt torque transient and the risk of irreversible demagnetization. Two permanent magnet traction motors, one with NdFeB magnets and the other with ferrite magnets, are considered, highlighting the pros and cons with reference to the safe state modes. Steady-state and transient operation under active short- and open-circuit conditions are swiftly evaluated for the existing designs using offline flux maps manipulation. Also, the influence of the magnet temperature on the safe turn-off is investigated. Finally, novel indexes are introduced and implemented on the (x, b) design plane, for the generalization of the results and the early evaluation of the safe state modes during the preliminary design of the machine.**

I. Introduction

A. Background

Nowadays, the electric traction market is dominated by internal permanent magnet (IPM) synchronous machines with NdFeB magnets [1] [2] [3]. Meanwhile, the scarcity and price instability of rare-earth materials are pushing the automotive industry towards alternative solutions [4]. Among these, the ferrite-assisted synchronous reluctance (PM-SyR) machines, already widely used in hybrid-electric drivetrains [5], are considered also for fully electrified axles [6]. However, the use of ferrite brings new design challenges since they are easy to demagnetize and have low remanence (i.e. reluctance torque must be ably exploited) [7].

Notably, in automotive applications, in case of loss of control of the inverter, two turn-off safe modes can be triggered: the active short-circuit (ASC) [8] or the inverter switches opening, namely open circuit (OC) strategy [9]. These two states offer opposite advantages and disadvantages and can lead to damage to the permanent magnets (PMs) [10] or to the inverter. Dealing with the ASC state, it ensures that no harmful voltage is present outside the motor, increasing safety and avoiding overvoltage on the inverter DC link as well as the Uncontrolled Generator Operation (UGO) [11]. However, ASC can produce high transient currents, exposing the motor to the risk of irreversible demagnetization of PMs and unsustainable shaft torques [12]. On the other hand, OC condition ensures that the motor is safe against demagnetization since no current circulates in it, but it poses the risk of dangerous voltages outside the motor, also higher than the DC link limit, with risk of UGO and inverter and battery damage. Indeed, the OC operation can be used only if the machine's back electromotive force (emf) is smaller than the DC link voltage, otherwise, the UGO arises. Further details on the turn-off safe strategies can be found in [13].

B. Paper organization and benchmark motors

Since the safe modes feasibility is a strict constraint that involves machine design [15], this paper proposes in Sections II and III an efficient technique to comprehensively evaluate the doable turn-off safe modes in the torque-speed domain; here, the PM temperature effect is also examined. Then, Section IV presents easy-to-evaluate indicators to contemplate the doable safe modes already in the preliminary design

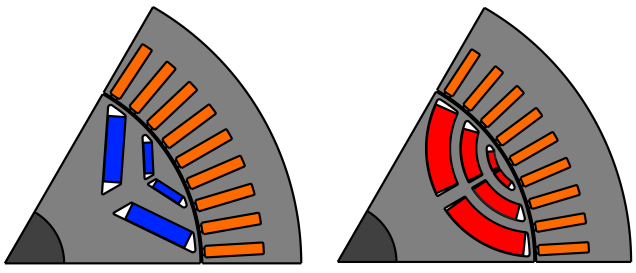

Fig. 1. Radial cross-section of the (a) IPM and (b) PM-SyR machines used as benchmarks [14].

TABLE I
MOTOR SPECIFICATIONS COMPARISON [14].

		IPM	PM-SyR	
Stator outer diameter	D	225	225	[mm]
Stack length	L	114	211	[mm]
Peak torque	T	444	437	[Nm]
Base power factor	$cos\varphi$	0.74	0.62	
Peak power	P	225	256	[kW]
Base speed	n_{base}	4845	5593	[rpm]
DC link voltage	V_{dc}	320	320	[V]
Peak phase current	I_{max}	1131	1556	[Apk]
Number of turns	N_s	18	9	

process; this is achieved by enforcing the design procedure showcased in [16] with new insights and analysis.

The two PM synchronous machines (PMSMs) used as benchmarks are a two-layer V-type IPM machine with NdFeB magnets and a PM-SyR machine with ferrite and circular flux barriers, indicated in the following respectively as IPM and PM-SyR. Their radial cross-sections are shown in Fig. 1, while their ratings are reported in Tab. I. Note that their design process is based on the target specifications of the 3D6 IPM motor of the Tesla Model 3 as presented in [14].
Last, all the procedures are part of the open-source Matlab-based project SyR-e, made freely available on GitHub [17].

II. MOTOR MODELLING FOR SAFE STATE OPERATIONS

In this section, the methodologies to compute the motor model, considering also the post-fault safe state operations, are described.
The most critical aspect of this evaluation is the fast and accurate model of the ASC, while the OC condition is quite easy to consider. For the ASC model, the estimation of the peak short-circuit current is first estimated using the hyper-worst-case (HWC) short-circuit current concept [12], this value is used to define the limits of the flux maps and to build a complete model in the current domain. Then, the flux maps are computed at the considered PM temperature with adjusted current limits. This strategy produces an accurate magnetic model of the motor for both healthy performance assessment and ASC computation. Last, the demagnetization limit of the PM is computed as a function of the PM temperature, in order to have all the information for the ASC state evaluation.

A. Hyper-worst case active short-circuit current

A simplified estimation of the ASC peak current is based on the assumption that no flux decay happens during the transient; this current is called hyper-worst case i_{HWC} since it is unattainable to have a higher peak current thanks to the flux decay. How far the hyper-worst case estimation is from the actual peak current is investigated in Section II-C.

The i_{HWC} can be identified on the flux maps as the intersection between the negative d axis and the contour of pre-fault flux linkage λ_{ini}. Moreover, the HWC current can be

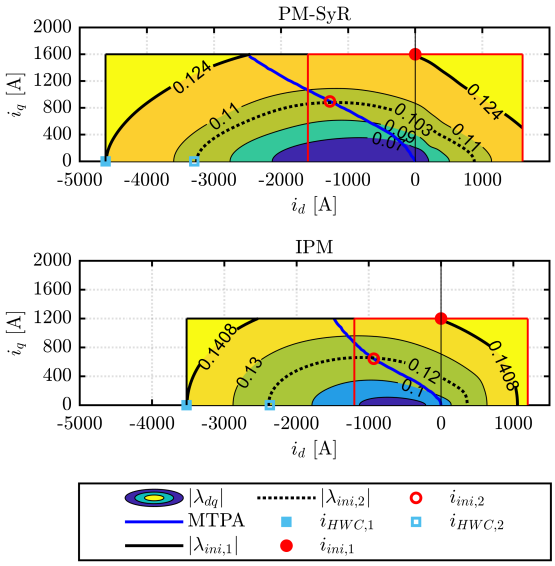

Fig. 2. Flux-linkage amplitude in the rectangular and two-quadrants square domain for the IPM and PM-SyR machines. The fault 1 starts from the maximum flux in the second quadrant and the fault 2 starts from the maximum current in MTPA condition.

easily computed without the flux maps information by means of an iterative process and FEA simulation, solving (1), as described in [12].

$$\lambda_d(i_{HWC}, 0) = -\lambda_{ini} \tag{1}$$

The i_{HWC} definition is shown in Fig. 2 for two pre-fault operating points: peak current in Maximum Torque Per Ampere (MTPA) condition (subscript 1), maximum current in q axis and zero current in the d axis (subscript 2). Also, the two λ_{ini} are reported with black contours and the pre-fault currents i_{ini} are identified with red circles.

Note that the fault with the subscript 2 has a significantly higher i_{HWC} since it is proportional to the pre-fault flux λ_{ini}. Furthermore, the fault 2 has the highest λ_{ini} in the second quadrants, thus it has the greatest i_{HWC} considering pre-faults in motoring operation. For this reason, it is used to define the d axis boundary of the rectangular current domain on the flux map computation, as presented in the following subsection.

B. Rectangular flux maps

To determine the ASC behaviour in the torque-speed domain, flux maps covering the HWC short-circuit currents are needed.

Usually, to evaluate the normal operation, flux maps with a square current domain are computed up to the maximum inverter current; an example of a two-quadrant square flux map is reported as a red grid in Fig. 3. However, to capture the ASC behaviour, wider flux maps in the PM axis are needed. Therefore, the d current negative limit of the grid is here found with the HWC current computed with the worst initial condition in the motoring quadrant. Note that the maximum

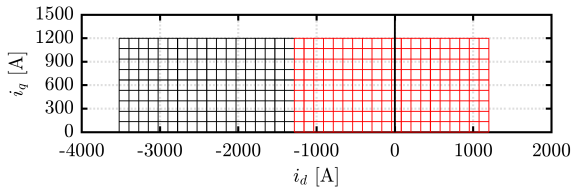

Fig. 3. In black, an example of a rectangular current grid for flux map computation; in red, a standard two-quadrant square flux map.

i_{HWC} corresponds to the maximum initial flux $\lambda_{ini,1}$, which is reached for $(i_d, i_q) = (0, I_{max})$, as addressed before. It follows that the current grid is extended in the d axis up to $i_{HWC,1}$, while the q axis limit is unchanged since no further data are needed at higher q currents. This results in a rectangular current grid that covers every i_{HWC} caused by an ASC starting from the motoring condition within the inverter current limit (Fig. 3). Also, note that with respect to a square current grid up to the maximum $i_{HWC,1}$, a rectangular domain permits minimizing the unused data and the computational time of the FEA flux map.

In Fig. 2, the initial pre-fault current, corresponding to the maximum flux amplitude in the motoring quadrant, and the related $i_{HWC,1}$ are reported with the subscript 1. Thus, the flux map is built by running FEA simulations along the current grid [18]; the resulting amplitude of the flux is displayed in Fig. 2. The maximum flux amplitude in the motoring quadrant, used to compute the $i_{HWC,1}$, is highlighted with a thicker black line.

Last, the rectangular flux maps are computed and post-processed as standard square maps, thus as disclosed in [18].

C. Current waveform during ASC

The HWC current estimates the peak current during an ASC transient, neglecting flux decay and leading to an over-estimation of the peak current. To accurately estimate the current waveform during an ASC, the motor magnetic model equations are solved, imposing zero voltage on both axes, as explained in [12].

The waveform computation needs the flux maps knowledge and it is based on the solution of differential equations in discrete form and on interpolation on the flux maps, thus it is more complex and time-consuming than the HWC current estimation.

The current waveform during an ASC is computed for both IPM and PM-SyR motors and the results are reported in Fig. 4. The considered pre-fault condition is the peak current along the MTPA, already defined with the subscript 2 in Fig. 2. The figures report the MTPA in bold blue line and the current trajectory in red line. The coloured points are respectively the initial current (red circle), the peak current during ASC (red square), the HWC current (light blue square) and the steady-state ASC current (green cross), which corresponds to the characteristic current [12].

The current trajectories in Fig. 4 highlight that the eccentricity of the iso-flux lines is proportional to the machine saliency,

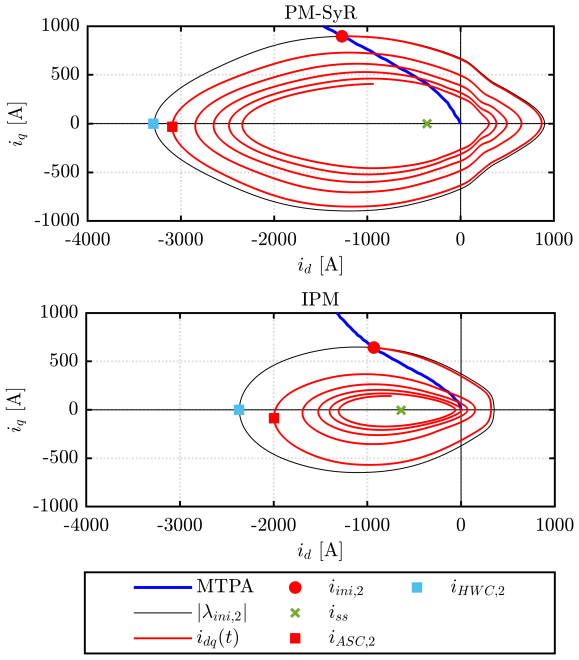

Fig. 4. Currrent trajectories during the short-circuit on the dq plane for the IPM and PM-SyR machines with the maximum inverter current in MTPA as pre-fault condition.

indeed the PM-SyR saliency is greater than the IPM one. Also, the i_{HWC} estimation is close to the actual maximum transient current, however, the first is retrieved instantaneously once the flux map is available while the latter is obtained in 3 minutes (with a workstation with Intel Xeon E5-2690 v4 CPU, 14 cores and 32GB RAM). Therefore, to map the torque-speed domain, the i_{HWC} estimation is used for the sake of computational time.

Note that, since the flux spiral is travelled clockwise, a pre-fault condition in the second quadrant (motor) or third quadrant (brake) means a longer or shorter path to reach the maximum current point, and thus a longer or shorter decay time. Indeed, starting from braking operation, the peak short circuit current is expected to be higher than from motoring due to less damping effect and therefore closer to the hyper-worst case estimation.

D. Demagnetizing current and UGO limits

To define whether the ASC state is safe or not, the irreversible demagnetization of the PMs must be investigated at the peak ASC current.

In order to speed up the computation process and avoid FEA simulation for each operating point [19], the demagnetization curve is computed. This curve reports the maximum demagnetizing current that does not irreversibly demagnetize the PMs (with a tolerance of 1% of the PM volume), a function of the PM temperature [20]. The demagnetization limit is computed by means of an iterative process and FEA simulations. During each iteration, a test current is imposed aligned against the PMs and the flux density in each mesh element of the PMs is compared with the knee point of the BH curve: if the FEA

flux density is lower than the knee point, the mesh element is considered irreversibly demagnetized.

The results for the two case studies are reported in Fig. 5; here, the demagnetizing currents are compared with the maximum inverter current. As expected, from the demagnetization point of view, the worst-case for the ferrite is at the lowest temperature, while the opposite happens for the NdFeB.

On the other hand, the UGO speed is more straightforward to define, since it can be retrieved analytically once the magnet flux is known:

$$n_{UGO} = \frac{V_{DC}}{\sqrt{3} \cdot p \cdot \lambda_m} \cdot \frac{30}{\pi} \tag{2}$$

where p is the number of pole pairs and V_{DC} is the DC voltage. Thus, Fig. 6 reports the n_{UGO} as a function of the PM temperature for the two benchmark motors. Comparing the n_{UGO} with the maximum motor speed n_{max}, it is possible to conclude that the IPM machine has an OC unsafe area within its torque-speed domain for every PM temperature, while the opposite happens for the PM-SyR machine thanks to its smaller PM remanence.

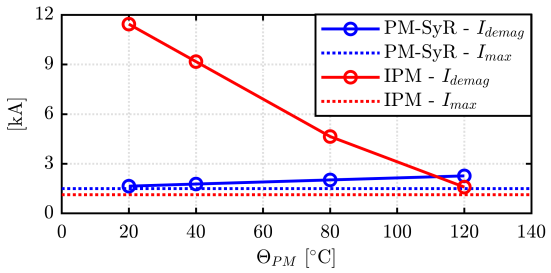

Fig. 5. Demagnetizing current limit at different PM temperatures for the IPM and PM-SyR machines. Note that the displayed currents demagnetize 1% of the total PM volume.

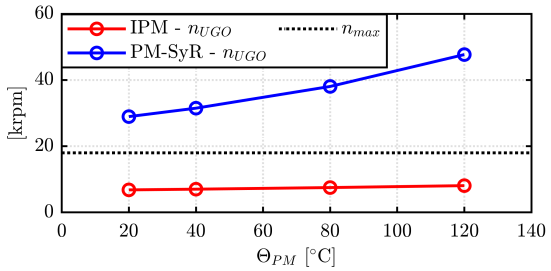

Fig. 6. UGO speed as function the PM temperature for the IPM and PM-SyR machines. The maximum speed is reported with a dotted black line.

III. Safe conditions in torque-speed domain

In this section, the doable safe modes are detected in the torque-speed domain, ensuring a safe turn-off in every working condition. Also, guidelines on how to deal with the PM temperature influence are provided.

A. ASC and OC modes evaluation

With the ASC mode, the motor terminals are closed together, making the voltage outside the motor equal to zero, without the risk of inverter and battery damage and avoiding harmful voltages. The main problem with this state is the peak transient short circuit current, which can irreversibly demagnetize the motor PMs, causing performance degradation. It follows that the ASC state can be defined as safe if the motor can withstand the peak transient short circuit current without irreversible demagnetization. Usually, the steady-state short-circuit current is not critical, since the system is stopped after the fault. Since the peak ASC current is a function of the pre-fault condition, every working point on the (T, n) plane is considered and the HWC short-circuit currents are computed in the (T, n) domain. The computation of the HWC current is used instead of the full transient solution, because of computational efficiency. Moreover, no further FEA simulations are performed and the HWC current is identified interpolating the pre-fault flux density contour with the negative d axis. In this way, the computation is instantaneous. Then, the HWC current is compared with the demagnetization current limit in all the (T, n) points: if the HWC current is higher than the demagnetization limit, the point is labelled as ASC unsafe and marked in red, as done for the PM-SyR in Fig. 7a. It is worth noting that the ASC safe points are the ones below a certain flux linkage, while the operating points in the low-speed/high torque region are unsafe for ASC, in the flux-weakening region, the ASC is less critical.

On the other hand, the OC mode is the dual of the ASC state. Indeed, in this case, the motor terminals are left open, making the phase current null. Therefore, the motor is safe, but possible problems can arise because of the no-load voltage of the motor. For a given pre-fault point, the OC state is defined as safe if the motor no-load voltage is lower than the rated motor voltage. This process is repeated for each (T, n) point, as done for the ASC state.

B. Safe modes evaluation on the PM-SyR machine

Considering the ASC operation, Fig. 5 conveys that the worst-case PM temperature occurs at the minimum considered temperature (20 °C). The same happens for the OC mode, as reported in Fig. 6, since at lower PM temperature the magnet flux is greater (2). Therefore, once a safe area is detected in the torque-speed domain for a PM temperature of 20 °C, this area is valid even for higher temperatures.

Thus, Fig. 7 investigates the safe areas for the ASC and OC modes with PMs at 20 °C. The ASC operation is unsafe for almost every working point lower than around 10500 rpm, while the OC mode is always safe. This happens because the demagnetizing current limit at 20 °C is very low (Fig. 5), thus most of the i_{HWC} in the torque-speed domain exceed this limit. On the other hand, the n_{UGO} at 20 °C falls beyond the maximum speed. Thus, in conclusion, for the PM-SyR machine, **the OC mode is identified as the optimal turn-off safe state mode** in every working condition in motor functioning.

Finally, for the sake of clarity, also the ASC safe area at the maximum PM temperature of 120 °C is reported (Fig. 8) to corroborate as already expressed: the ASC safe area increases with a PM temperature growth for ferrite machines.

C. Safe modes evaluation on the IPM machine

The NdFeB-based machine has an opposite trend on the ASC mode with respect to the PM temperature as highlighted in Fig. 5. It follows that there is not a unique worst-case PM temperature, since, the demagnetizing current limit is lower at higher temperatures (i.e. smaller ASC safe areas); while, according to Fig. 6, the n_{UGO} is lower at reduced temperatures (i.e. smaller OC safe areas). Therefore, here a precautionary approach is applied: each turn-off safe state is assessed at its respective worst-case PM temperature. Indeed, Fig. 9 reports the ASC safe area at 120°C and the OC safe area at 20°C. According to Fig. 9, it is not possible to define a unique safe mode valid for every working point in the torque-speed domain, however, every point has at least one doable safe mode. For these reasons, a **hybrid strategy** can be adopted: **OC mode for speeds lower than 6500 rpm and ASC mode for higher speeds**.

Finally, as done for the PM-SyR machine, the ASC safe area at the antagonistic PM temperature is shown to highlight the temperature effect. As expressed, the ASC safe area for NdFeB-based machines is widened for lower PM temperatures. In this case, at 20°C, the demagnetizing current limit is strongly increased to a value equal to around 11 times the maximum inverter current (Fig. 10), therefore, in every working point the i_{HWC} do not reach such an extensive value and thus the ASC mode becomes always safe.

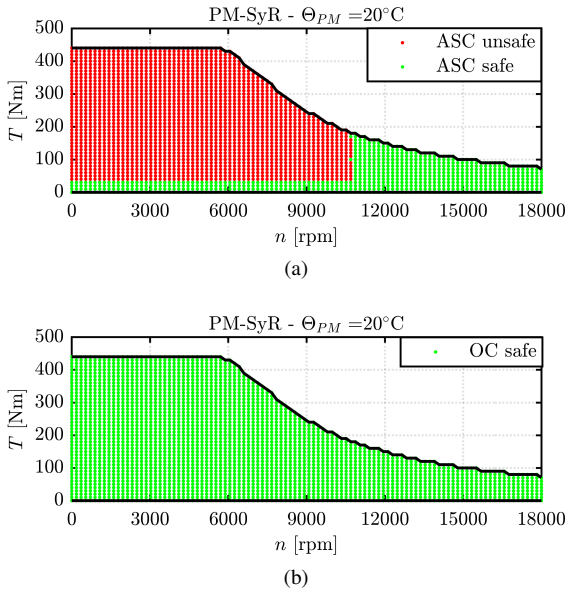

Fig. 7. Safe areas of the PM-SyR machine with PM at 20°C: (a) ASC and (b) OC modes.

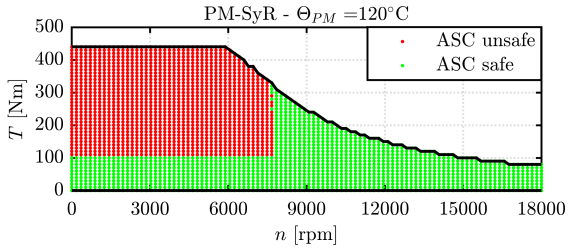

Fig. 8. ASC safe area of the PM-SyR machine with PM at 120°C.

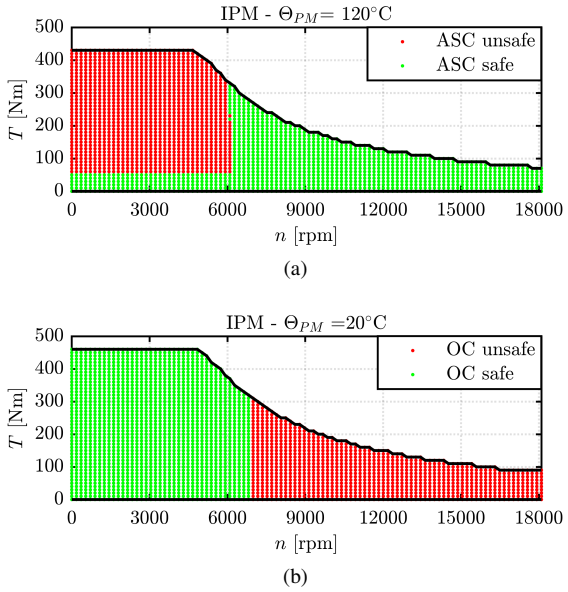

Fig. 9. Safe areas of the IPM machine: (a) ASC mode with PM at 120°C and (b) OC mode with PM at 20°C.

IV. Novel Figures of Merit on the Design Plane

A. The (x, b) design plane

The (x, b) design plane is used to quickly determine the motor cross-section, given the dimensional, electrical, magnetic, thermal and maximum speed constraints [16]. The two design plane variables are x and b, which represent the ratio between rotor and stator diameter and between airgap and iron flux density, respectively. Thanks to design equations, each (x, b) point represents a different cross-section; in this way, a large number of performance figures can be visualised directly on the design plane for a continuum of candidate machines. The design plane is built and computed with an analytical model and design equations. Moreover, a few FEA simulations are adopted to correct the analytical model, in the so-called FEAfix process [21]. Note that the design planes are built at a constant current density to ensure similar thermal behaviour and the displayed performance is obtained in MTPA at peak current (maximum inverter current). More details about the (x, b) design plane can be found in [16].

Considering the case studies ratings, the design planes are built and the torque and power factor trends are reported in Fig. 11. Contemplating the other figures of merit (number of turns and inverter ratings), the coordinates of the two motors

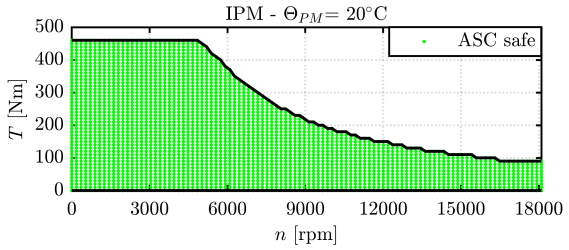

Fig. 10. ASC safe area of the IPM machine with PM at 20°C.

were selected, as disclosed in detail in [14]. In the following, the design planes are enriched with novel figures of merit to evaluate the doable safe modes.

B. New indexes for safe state modes

The choice of the number of turns to meet the inverter ratings and the basic design requirements (torque and power factor) are already covered in literature [16] [14]. Here, the focus is on the safe states evaluation: the ASC and OC states are assessed by means of novel indexes added to the preliminary design process. For this aim, the indexes are defined in such a way that they are independent of the number of turns as described in the following. Also, note that the planes refer to a PM temperature of 80°C.

Given the current I, function of the (x, b) coordinated and fixed by the constant current density along the plane, the peak current during an ASC transient is assessed with the ratio i_{HWC}/I. In every FEAfix point, iterative FEA simulations are run to retrieve the i_{HWC}, thus, the percentage of demagnetized PM volume at i_{HWC} is computed and the percentage of demagnetized PM saved. As done before, the ASC operation is deemed feasible if less than 1% of PM is demagnetized. From Fig. 12, it can be noted that the peak currents during an ASC are slightly higher for the IPM machine than the PM-SyR, because of the higher PM content (higher steady-state short circuit). However, the IPM plane results in having almost zero demagnetized motors at its i_{HWC}/I, while for the PM-SyR plane 100% of the motors suffer from demagnetization. This communicates that even if the two planes have similar

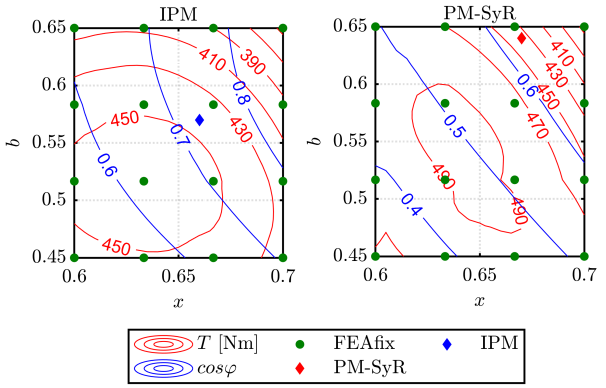

Fig. 11. Design planes with the torque and power factor contours for the IPM and PM-SyR machines.

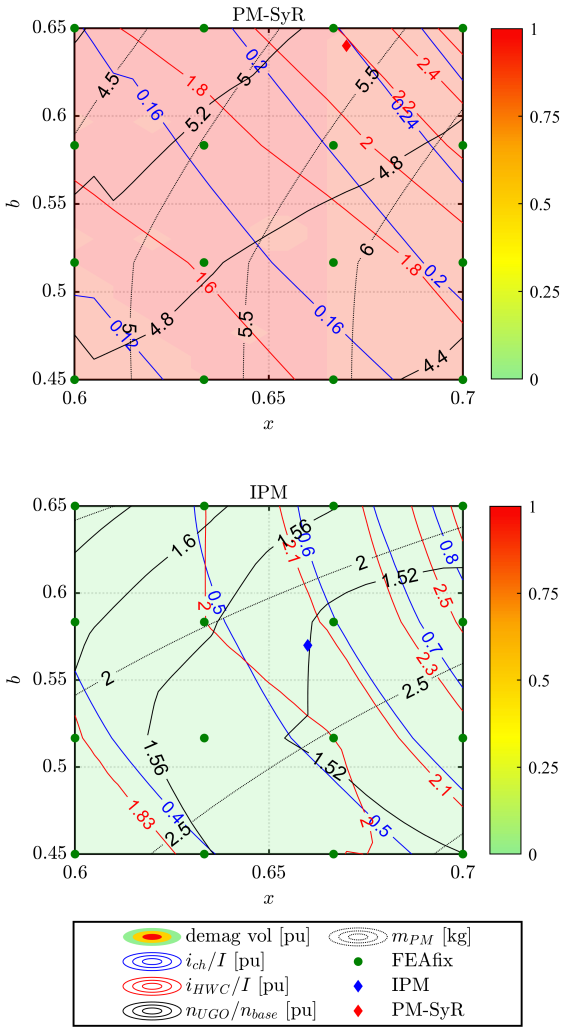

Fig. 12. Design planes of the PM-SyR and IPM machines with indexes on ASC and OC states.

i_{HWC}, for the IPM machine the ASC can be triggered in MTPA and peak current condition for every (x, b) design, while for the PM-SyR machine is valid the opposite. These findings match the analysis reported in Fig. 7a, where the PM-SyR, at corner speed and peak current, is unsafe with respect to the ASC. Moreover, the ferrite design plane demonstrates that even changing the machine geometry, it is unfeasible to achieve a safe ASC at peak current/corner speed; whilst, all the opposite happens for the IPM motor.

Dealing with the UGO limit, it is evaluated as the ratio between the UGO and base speeds, respectively n_{UGO} and n_{base}. The latter depends on the machine flux at the MTPA maximum inverter current λ_{MTPA}, which is the working point evaluated along the design plane.

$$n_{base} = \frac{V_{DC}}{\sqrt{3} \cdot p \cdot \lambda_{MTPA}} \cdot \frac{30}{\pi} \tag{3}$$

Therefore, from (2) and (3), it can be found the ratio between the UGO and base speed (4), which does not depend on the number of turns.

$$\frac{n_{UGO}}{n_{base}} = \frac{\lambda_{MTPA}}{\lambda_m} \tag{4}$$

Note that the defined ratio (4) strongly depends on the magnet flux; therefore, as expected, the Fig. 12 shows that the NdFeB plane has a significantly lower UGO speed than the ferrite plane. According to the ratings, the maximum speed and base speed ratio is equal to 3.8. In Fig. 12, it can be noted that the UGO limit in the PM-SyR plane always exceeds the 3.8 target, whilst the opposite results for the IPM machine. Thus, as for the ASC mode, also the OC mode feasibility can be directly assessed from the design plane during the preliminary design since it is able to forecast some of the results shown in Section III, namely the OC safety limit and the ASC safety at maximum MTPA current.

V. Conclusion

This paper presents an analysis of the safe states of PM motors, carried out on two motors, one with NdFeB PMs and the other with ferrite PMs. First, it is exhibited how to collect all the needed data to deal with the safe state evaluation. Then, for each motor, the safety of two turn-off states, ASC and OC, is evaluated in the torque-speed domain considering the worst-case PM temperature. Thus, the best turn-off strategy is selected: the ferrite machine can rely on the OC operation in every working condition, mainly thanks to its lower magnet flux, while the NdFeB machine does not have a unique safe mode for every working condition. Indeed, the latter can achieve a safe turn-off with an hybrid strategy: for speeds lower than 6500, the OC state can be exploited, whilst for higher speeds the ASC state must be triggered. Also, the PM temperature effect on the safe areas is investigated and commented. Finally, new indexes are added to the (x, b) design plane formulation, enabling the evaluation of the two turn-off safe modes at the very early design steps, as well as an in-depth understanding of the machine parameters that influence the safety of the turn-off modes.

Acknowledgment

The research has been conducted with the support of Power Electronics Innovation Center (PEIC) of Politecnico di Torino.

References

[1] C. S. Goli, M. Manjrekar, S. Essakiappan, P. Sahu, and N. Shah, "Landscaping and Review of Traction Motors for Electric Vehicle Applications," in *2021 IEEE Transportation Electrification Conference & Expo (ITEC)*, Jun. 2021, pp. 162–168, iSSN: 2377-5483.

[2] A. Krings and C. Monissen, "Review and Trends in Electric Traction Motors for Battery Electric and Hybrid Vehicles," in *2020 International Conference on Electrical Machines (ICEM)*, vol. 1, Aug. 2020, pp. 1807–1813, iSSN: 2381-4802.

[3] I. Husain, B. Ozpineci, M. S. Islam, E. Gurpinar, G.-J. Su, W. Yu, S. Chowdhury, L. Xue, D. Rahman, and R. Sahu, "Electric Drive Technology Trends, Challenges, and Opportunities for Future Electric Vehicles," *Proceedings of the IEEE*, vol. 109, no. 6, pp. 1039–1059, Jun. 2021.

[4] J. D. Widmer, R. Martin, and M. Kimiabeigi, "Electric vehicle traction motors without rare earth magnets," *Sustainable Materials and Technologies*, vol. 3, pp. 7–13, Apr. 2015. [Online]. Available: https://www.sciencedirect.com/science/article/pii/S2214993715000032

[5] S. Jurkovic, K. Rahman, B. Bae, N. Patel, and P. Savagian, "Next generation chevy volt electric machines; design, optimization and control for performance and rare-earth mitigation," in *2015 IEEE Energy Conversion Congress and Exposition (ECCE)*, Sep. 2015, pp. 5219–5226, iSSN: 2329-3748.

[6] S. Morimoto, S. Ooi, Y. Inoue, and M. Sanada, "Experimental Evaluation of a Rare-Earth-Free PMASynRM With Ferrite Magnets for Automotive Applications," *IEEE Transactions on Industrial Electronics*, vol. 61, no. 10, pp. 5749–5756, Oct. 2014.

[7] Y. Hu, H. Wei, H. Chen, B. Zhou, X. Zhu, H. Zhang, P. Xu, and L. Li, "Research on Demagnetization Mechanism and Test Method of Ferrite Permanent Magnet Assisted Synchronous Reluctance Motor," in *2019 22nd International Conference on Electrical Machines and Systems (ICEMS)*, Aug. 2019, pp. 1–4, iSSN: 2642-5513.

[8] A. Ruiz, A. Meseamanolis, L. Santolaria, M. Maleki, and A. Baschnagel, "Active Short Circuit Capability of HalfBridge Power Modules Towards EMobility Applications," in *PCIM Europe digital days 2021; International Exhibition and Conference for Power Electronics, Intelligent Motion, Renewable Energy and Energy Management*, May 2021, pp. 1–7.

[9] A. Akay, P. Lefley, and M. Kansara, "Open-Circuit Fault-Tolerant Control for a Five-Phase Permanent Magnet Synchronous Machine Drive," in *2020 7th International Conference on Electrical and Electronics Engineering (ICEEE)*, Apr. 2020, pp. 150–154.

[10] W. Peng, W. Kun, and F. Meng, "Demagnetization Study of Permanent Magnet Machine Under Three Phase Short Circuit," in *2023 IEEE 6th International Electrical and Energy Conference (CIEEC)*, May 2023, pp. 2705–2710.

[11] T. Jahns and V. Caliskan, "Uncontrolled generator operation of interior PM synchronous machines following high-speed inverter shutdown," *IEEE Transactions on Industry Applications*, vol. 35, no. 6, pp. 1347–1357, Nov. 1999.

[12] S. Ferrari, G. Dilevrano, P. Ragazzo, P. Pescetto, and G. Pellegrino, "Fast Determination of Transient Short-Circuit Current of PM Synchronous Machines via Magnetostatic Flux Maps," *IEEE Transactions on Industry Applications*, vol. 59, no. 4, pp. 4000–4009, Jul. 2023.

[13] A. R. Chandran, M. D. Hennen, A. Arkkio, and A. Belahcen, "Safe Turn-Off Strategy for Electric Drives in Automotive Applications," *IEEE Transactions on Transportation Electrification*, vol. 8, no. 1, pp. 9–22, Mar. 2022.

[14] G. Dilevrano, P. Ragazzo, S. Ferrari, and Pellegrino, "Comparative Design of Ferrite- and NdFeB- PMSMs using the (x,b) Design Plane," in *International Electric Machines and Drives Conference (IEMDC)*, San Francisco, USA, May 2023.

[15] G. Pellegrino, A. Vagati, and P. Guglielmi, "Design Tradeoffs Between Constant Power Speed Range, Uncontrolled Generator Operation, and Rated Current of IPM Motor Drives," *IEEE Transactions on Industry Applications*, vol. 47, no. 5, pp. 1995–2003, Sep. 2011.

[16] P. Ragazzo, G. Dilevrano, S. Ferrari, and G. Pellegrino, "Design of IPM Synchronous Machines Using Fast-FEA Corrected Design Equations," in *2022 International Conference on Electrical Machines (ICEM)*, Sep. 2022, pp. 1–7, iSSN: 2381-4802.

[17] G. Pellegrino and F. Cupertino, "SyR-e." [Online]. Available: https://github.com/SyR-e

[18] S. Ferrari, P. Ragazzo, G. Dilevrano, and G. Pellegrino, "Flux and Loss Map Based Evaluation of the Efficiency Map of Synchronous Machines," *IEEE Transactions on Industry Applications*, vol. 59, no. 2, pp. 1500–1509, Mar. 2023.

[19] K.-C. Kim, S.-B. Lim, D.-H. Koo, and J. Lee, "The Shape Design of Permanent Magnet for Permanent Magnet Synchronous Motor Considering Partial Demagnetization," *IEEE Transactions on Magnetics*, vol. 42, no. 10, pp. 3485–3487, Oct. 2006.

[20] S. Ruoho, J. Kolehmainen, J. Ikaheimo, and A. Arkkio, "Interdependence of Demagnetization, Loading, and Temperature Rise in a Permanent-Magnet Synchronous Motor," *IEEE Transactions on Magnetics*, vol. 46, no. 3, pp. 949–953, Mar. 2010.

[21] S. Ferrari and G. Pellegrino, "FEAfix: FEA Refinement of Design Equations for Synchronous Reluctance Machines," *IEEE Transactions on Industry Applications*, vol. 56, no. 1, pp. 256–266, Jan. 2020.